applied sciences

MDPI

Article

Thermal Response of Magnetic Refrigerants: Combined Effect of Temperature Dependent Specific Heat and Thermal Conductivity

Antonio P. Lopes [1,*], Vitor A. F. Costa [2] and Joao S. Amaral [1]

[1] Department of Physics, CICECO–Aveiro Institute of Materials, Campus Universitário de Santiago, University of Aveiro, 3810-193 Aveiro, Portugal; jamaral@ua.pt
[2] Department of Mechanical Engineering, Center for Mechanical Technology and Automation, Campus Universitário de Santiago, University of Aveiro, 3810-193 Aveiro, Portugal; v.costa@ua.pt
* Correspondence: antonio.lopes@ua.pt; Tel.: +351-234-370-200

Abstract: Device optimization plays a paramount role in current research on magnetic refrigeration. Solid state refrigerants have been characterized and numerical simulations assume a critical relevance in the development of magnetocaloric technology to have alternatives to vapour-compression systems whose operating elements have high global warming potential. Experimental studies have shown that the thermal properties of several magnetocaloric materials considerably change around their Curie temperatures (T_C) and that this temperature dependency should not be dismissed. Current numerical research does not fully predict the complete thermal response of such materials, due to inaccuracies from neglecting the impact of combining both thermal conductivity (k) and specific heat (C_p) dependence on temperature. In this study, a simple unidimensional model includes $k(T)$ and $C_p(T)$ functions as input parameters, highlighting the relevance of considering temperature dependent thermophysical properties' inputs when simulating the magnetic refrigerant's heat transfer processes. The obtained results evidence that neglecting the temperature dependence of the magnetocaloric material thermophysical properties, namely its thermal conductivity and its specific heat, affects its temperature response, what may strongly affect the results after a succession of (hundreds or thousands) cycles.

Keywords: heat transfer; numerical modelling; thermophysical properties; thermal conductivity; magnetocaloric materials; temperature dependence

Citation: Lopes, A.P.; Costa,V.A.F.; Amaral, J.S. Thermal Response of Magnetic Refrigerants: Combined Effect of Temperature Dependent Specific Heat and Thermal Conductivity. *Appl. Sci.* **2022**, *12*, 6581. https://doi.org/10.3390/app12136581

Academic Editor: Jacek Tomków

Received: 19 May 2022
Accepted: 20 June 2022
Published: 29 June 2022

1. Introduction

Thermal management of spaces is, historically, one of humankind's largest energy uses. Nowadays, the combined end-use expenditure for regulating household temperatures, ranging from water heating to refrigeration represent over 50% of domestic and commercial building energy consumption [1,2]. Access to affordable, reliable and sustainable energy for all, remains one of the crucial United Nations' goals for the upcoming decades. Any sizable efficiency increase on thermal management technology will have a huge impact in worldwide environment and economics [3]. The development of novel caloric devices aims to replace the traditional vapor-compression refrigeration and heat pumping technology, which have low efficiencies and use non-renewable resources [4]. In that respect, for the past two decades, Magnetocaloric (MC) systems have been the most studied caloric field [5].

Magnetic refrigerators and heat pumps are based on porous-like structures made of magnetocaloric materials (MCM), most commonly assembled as parallel plate arrays or packed spheres [6]. These magnetocaloric matrices are cyclically subject to applied magnetic field changes, where the temperature of the solid-state refrigerant varies due to magnetic alignment and subsequent entropy changes. This intrinsic Magnetocaloric Effect (MCE) is maximized in the vicinity of magnetic phase transitions, particularly near the

Curie temperature (T_C), such that if the MCM is demagnetized adiabatically its temperature decreases [7].

MC devices take advantage of these sharp changes on the refrigerant's thermodynamic properties and exploit them in the most efficient thermodynamic cycle. The MC system usually is made of field generating magnets, a porous regenerator made of a chosen MCM, a fluid pumping system, and heat exchangers (HEX) [8]. Combining the aforementioned MC cycle, along with the Heat Transfer Fluid (HTF) oscillation, a temperature difference is created between the heat exchangers [9]. For example, Gadolinium (Gd), the most common MCM used in MC prototypes (T_C around 294 K), can display a maximum adiabatic temperature span (ΔT_{ad}) of approximately 5.5 K, when subject to an applied magnetic field from 0 to 2 T [10].

Active magnetic regenerators (AMR) were developed and adopted, in every type of MC device, to bypass the material's low ΔT_{ad}, promoting larger heat storage capacities on both opposite heat sinks. As the energy transfer increases due to a larger temperature span, in each magnetic cycle, the HTF transfers larger heat loads between the magnetocaloric material and the heat exchangers. In the AMR cycle, the MCM's heat capacity acts as a dynamic regenerator, absorbing or releasing heat into the HTF, actively creating a heat regenerative ensemble throughout the process [11]. One of the main goals of the regenerator is to extract as much thermal energy as possible from the magnetized active volume while still having excellent heat transfer towards the HTF. To optimize such operation, AMR numerical models are created to help reduce the uncertainty of the next generation prototypes' performance. Some examples can be found in recent years in which numerical models are used to predict and improve the efficiency of MC regenerators when small variations are introduced in one specific aspect of the device [12–14].

Modelling becomes an essential tool for designing improved thermomagnetic devices, reducing the number of fully developed prototypes needed to reach high performance magnetocaloric systems. In the literature, most numerical models use a 1D approach because of its simplicity and low computational requirements [15]. These types of model are easy to make, modify and adapt, but they are less accurate. 1D models usually neglect the interface thermal conduction and require the use of a heat-transfer coefficient between the fluid and the solid matrix. Despite the larger computational cost, 2D models have also been considered, mainly used when dealing with slow heat transfer processes along the perpendicular flow direction, where the modelled fluid cannot transport the heat completely within one cycle [16]. Regarding the 3D models developed so far, the computational resources were so high that in order to model a complete MC regenerator, Bouchard et al. (2009), only computed a few magnetocaloric cycles [17]. In other cases, authors adopt different strategies to reduce the computing power cost, required by the designed models. For example Kamran et al. (2016) only modelled one MC microchannel regenerator instead of a complete structure [18]. Mugica et al. (2018) divided the model into two so that the fluid dynamics (3D) could be computed separately from the heat transfer process (1D) [19].

Silva et al. (2021) compiled several published MC numerical models, classifying them by the degree to which the underlying physical phenomena are solved and implemented [20]. Each physical property used in MC models depends on parameters like temperature T and magnetic field H. In MCM numerical modelling, the use of these two dependencies in the literature presents itself considerably divergent. Recent models all use temperature dependent specific heat ($C_p(T)$) domains, whether it has been calculated through Mean Field Theory (MFT) or obtained experimentally [21–23]. $C_p(T)$ is required to have a thermodynamic sound model [24]. Nevertheless, some models have used a constant C_p approximations [25,26]. These intrinsic thermal properties, like C_p and k are in the genesis of specific energy transfer mechanisms. To more accurately evaluate the overall contributions to heat transfer, C_p and k temperature dependence should be accounted for in numerical simulations [27], not only because it is a closer representation of actual physical conditions but also to provide better predictive solutions.

Concerning thermal conductivity k, Nielsen et al. (2012) demonstrated that large operating frequencies demand large k, and small operating frequencies demand small k, when simulating a complete AMR regenerator [28]. So far, Silva et al. (2019) developed the only AMR numerical model that employs temperature dependent k [29]. The research group concluded that changing k approximately by 50% within a temperature window of 10 K, can significantly impact the overall AMR cycle's performance. This result may be approximated to actual values in some cases since Fujieda et al. (2004) already had measured a 10% change in thermal conductivity across a 20 K window near room temperature for some MC materials [30], which can influence the time constant temperature change during the MCE [31]. Despite that, nowadays, predictive algorithms already can provide reliable and accurate MCM $C_p(T)$ input values [32], the same cannot be said for the material's k, which is still considered immutable [23,33–35].

As pointed out in this introduction, plenty of AMR numerical models have been developed in the past. However, the accuracy of these models can be improved by considering temperature dependent properties. Silva et al. (2019) successfully incorporated $k(T)$ values into a magnetocaloric device model [29]. Nevertheless, in this paper, a deeper scrutiny is made on the heat transfer dynamics of a idealized MCM slab, detailing the impact of implementing more than one temperature dependent physical property. The main objective is to fill a gap in the literature by understanding specifically how the inclusion of $C_p(T)$ and $k(T)$, in a completely controlled numerical environment, can influence the heat transfer process, highlighting the relevance of the thermal conductivity's temperature dependence on magnetocaloric materials. For this purpose, a 1D mathematical heat transfer model has been developed to simulate a simple cool-down process in a single Gd stage near-room temperature and study the impact of changing its thermal properties over time on its dynamics.

The 1D model is intentionally simple, displaying these effects in a single cool-down step instead of the complete AMR cycling process period. The developed code grants the user full control over its inputs and resolution parameters, contrasting with commercial software packages, which can be restrictive, e.g., when freedom to take a step back or diverge from the preconceived source code is required. Despite their extensive material databases, these simulation software suites present unknown temperature dependent properties characterization for the chosen temperature ranges when dealing with caloric materials (CM).

This study explores the implications of integrating temperature dependent thermal properties and investigates their influence on the thermal response dynamics of a magnetocaloric material. These implications can undoubtedly affect the dynamics of the complete AMR systems, which can compromise the model's predicted performance. However, it matters noting that the study of these complete systems is out of this paper's scope.

2. Physical Model

The considered 1D model consists of a gadolinium slab with thickness L, thermally insulated on all sides except one, allowing horizontal heat flow into an idealized isothermal external medium. The slab starts the process at T_i = 320 K, and cools down until it reaches a steady-state temperature of T_∞ = 260 K (external medium temperature), assuming a constant convection heat transfer coefficient of h = 1100 W m^{-2} K^{-1} (typical free convection coefficient value for water).

We've explicitly derived a discretization of the spatial nodal temperature from the energy balance equation. The nodal temperatures of each designated surface point were obtained using Equations (1)–(3), for each time instant $\boldsymbol{t + n}\Delta t$, starting from $\boldsymbol{t}$, where $\boldsymbol{n}$ represents the time index and $\boldsymbol{n + 1}$ the next instant. As the slab cools down, it releases heat to the external surroundings triggering fluctuations in both temperature dependent C_p and k, along the material's control volume nodes.

Node 1:

$$T_1^{(n+1)} = \left[\frac{2k_{12}\Delta t}{\rho_1 C_1 \Delta x^2}\right] T_2^n + \left[1 - \frac{2k_{12}\Delta t}{\rho_1 C_1 \Delta x^2} - \frac{2h\Delta t}{\rho_1 C_1 \Delta x}\right] T_1^n + \left[\frac{2h\Delta t}{\rho_1 C_1 \Delta x}\right] T_\infty \quad (1)$$

Node 2:

$$T_2^{(n+1)} = \left[\frac{k_{12}\Delta t}{\rho_2 C_2 \Delta x^2}\right] T_1^n + \left[\frac{k_{23}\Delta t}{\rho_2 C_2 \Delta x^2}\right] T_3^n + \left[1 - \frac{k_{12}\Delta t}{\rho_2 C_2 \Delta x^2} - \frac{k_{23}\Delta t}{\rho_2 C_2 \Delta x^2}\right] T_2^n \quad (2)$$

Node 3:

$$T_3^{(n+1)} = \left[\frac{k_{23}\Delta t}{\rho_3 C_3 \Delta x^2}\right] T_2^n + \left[1 - \frac{k_{23}\Delta t}{\rho_3 C_3 \Delta x^2}\right] T_3^n \quad (3)$$

where T is the temperature in each spatial node, h the heat transfer coefficient, ρ the material's density, C the specific heat, k the thermal conductivity, and Δx represents the control volume length. To determine thermal conditions more accurately near the surface, the system's outer node 1 (the interface point between the slab and the external medium shown in Figure 1) has been assigned to the control volume with thickness of $\left(\frac{\Delta x}{2}\right)$. This control volume acts as a gateway for all the internal heat flowing outwards.

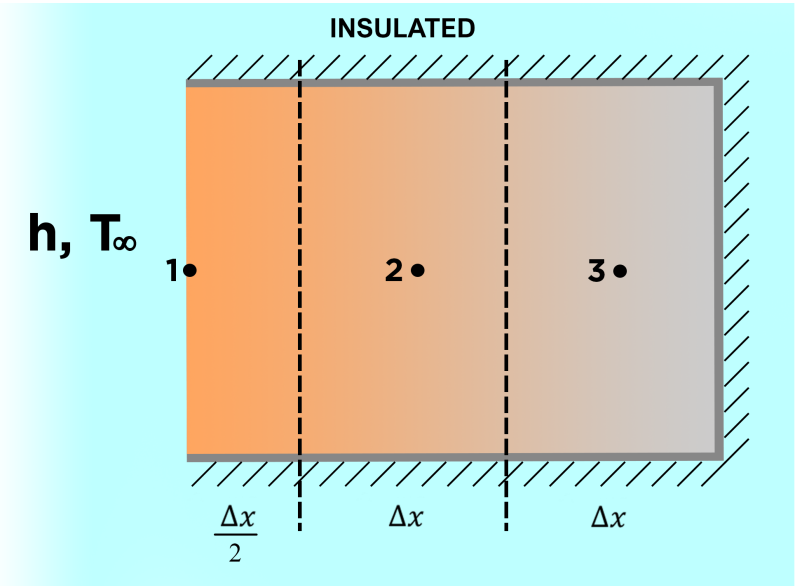

Figure 1. System's geometry, composed by a piece of Gd and an idealized surrounding. The 1D model assumes a heat flux path that begins inside the MCM and extends outwards along the line that intercepts the control volumes associated to nodal points 3, 2 and 1.

Temperature Dependent Physical Properties

The mathematical model introduces both temperature dependent $C_p(T)$ and $k(T)$ functions in order to see the differences in internal nodal heat transfer at the boundary interface. As heat flows outwards across fixed distances, average thermal conductivities between nodes (k_{12} and k_{23}), were evaluated through the harmonic mean approximation

(Equations (4) and (5)), that correspond to the effective thermal conductivity values at the interfaces between the adjacent control volumes 1 and 2, and 2 and 3, respectively:

$$k_{12} = \left[\frac{2k_1k_2}{k_1 + k_2}\right] \tag{4}$$

$$k_{23} = \left[\frac{2k_2k_3}{k_2 + k_3}\right] \tag{5}$$

Temperature dependent thermal conductivity inputs have been adapted from Silva et al. (2019) [29], as shown in Figure 2, where $k(T)$ values change between 8.4 and 12.6 W m^{-1} K^{-1}. A near-room temperature value of 295 K was used to numerically trigger sudden changes in the material's thermal conductivity, whether the simulated behaviour is increasing or decreasing on temperature. The $k(T)$ dependencies can be described as:

1. ***kGd***—constant k = 10.5 W m^{-1} K^{-1}, equal to the thermal conductivity of Gd at 293 K;
2. ***k(T)minus***—decreasing k while temperature increases;
3. ***k(T)plus***—increasing k while temperature increases.

The chosen values for C_p and ρ were adapted from Petersen et al. (2008) [36]. While ρ is kept constant at 7900 kg/m^3 throughout the entire slab's surface ($\rho_1 = \rho_2 = \rho_3$), the chosen specific heat values were linearly interpolated from data shown in Figure 3. The Curie temperature is highlighted with a vertical black line at T_c = 293.4 K, around which $C_p(T)$ suffers a sharp increase from 174.12 to 302.06 J kg^{-1} K^{-1}, when the material's temperature is decreasing.

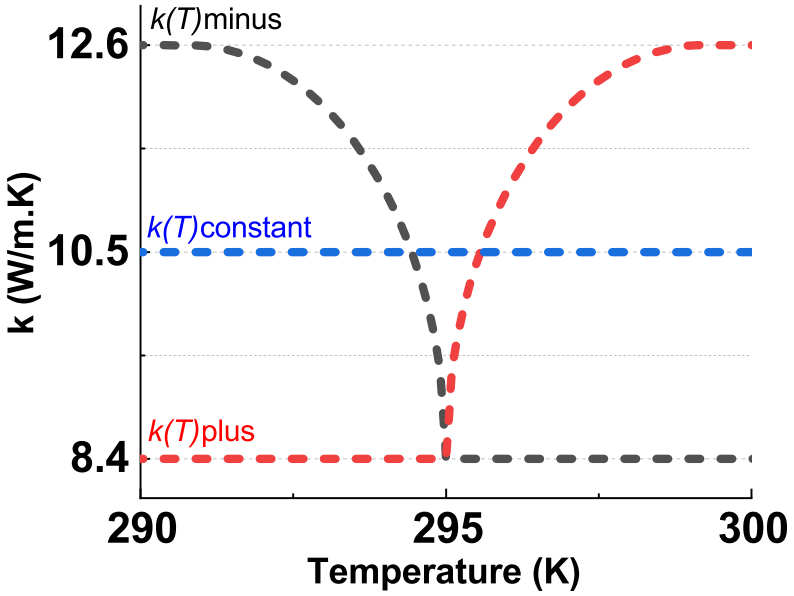

Figure 2. Three distinct $k(T)$ dependencies: ***kGd***—dash blue line; ***k(T)plus***—dashed red line; ***k(T)minus***—dash black line. Adapted from Silva et al. (2019).

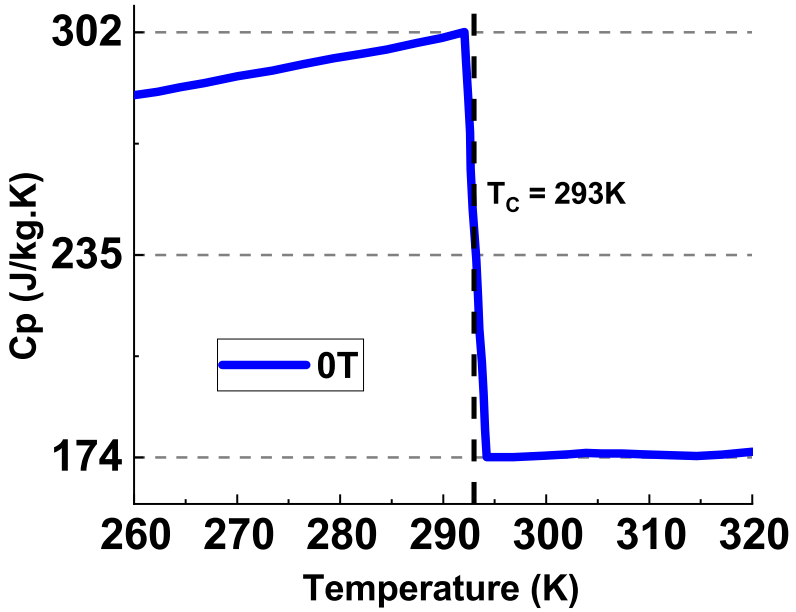

Figure 3. The heat capacity of gadolinium as a function of temperature in zero magnetic field. Adapted from Petersen et al. (2008).

3. Model Validation

3.1. Numerical Stability

The accuracy of our mathematical model solution depends on the number of interior nodal points and the number of time intervals required to carry the computation until the end. This accuracy increases with a decreasing Δt. The chosen length for each control volume is $\Delta x = \frac{2L}{5}$, with $L = 1$ mm, the typical thickness for a Gd parallel plate of a magnetocaloric regenerator [37,38]. For each Δx, the value of Δt has to be set to meet prescribed stability requirements [39]. The Δt value must be maintained below a specific limit, which requires that the nodal coefficients at the previous time instants must be greater than or equal to zero:

1. $\left[1 - \frac{2k_{12}\Delta t}{\rho_1 C_1 \Delta x}^2 - \frac{2h\Delta t}{\rho_1 C_1 \Delta x}\right] \geq 0$, for T_1^n coefficient;
2. $\left[1 - \frac{k_{12}\Delta t}{\rho_2 C_2 \Delta x^2} - \frac{k_{23}\Delta t}{\rho_2 C_2 \Delta x^2}\right] \geq 0$, for T_2^n coefficient;
3. $\left[1 - \frac{k_{23}\Delta t)}{\rho_3 C_3 \Delta x^2}\right] \geq 0$, for T_3^n coefficient.

A Δt value of 1 ms meets the stability criterion for every considered scenario.

3.2. Discharged Thermal Energy

The nodal temperature equations for each Δt compute the transient energy transfer process into the external medium. The model's energy conservation has been validated by analyzing the released heat through the outer boundary. All released energy must go through all control volumes, meaning that the last passing segment $V1$, relates directly to the boundary point 1. The nodal discharged energy is given by:

$$\Delta E = \rho_1 . V_1 . C_1 (T^{n+1} - T^n) \quad (6)$$

Two test cases were simulated to validate the model, comparing the slab's thermal response for the constant and temperature dependent scenarios, during 100 s. Both cases start with the same energy storage capacity. The initial specific heat values were set to $C_p = C_p(320\,\mathrm{K})$ and the thermal conductivity was fixed at $10.5\,\mathrm{W\,m^{-1}\,K^{-1}}$.

The total accumulated thermal energy has a value of 105.6 mJ and it is fully discharged in 15 s (ΔE) into the exterior, allowing the heat transfer system to reach (and remain) at steady-state conditions.

4. Results

A numerical simulation framework was developed to study the system's thermal response at the slab's surface. For an overall understanding of the system kinetics, the nodal temperature equations were solved for three different initial C_p values when running the constant physical properties scenarios (control group data), listed in Table 1. The C_p values represent the minimum, mean and maximum values taken from Figure 3. These control group simulations were then compared against five temperature dependent trials:

1. $C_p(T)$, $k = 10.5\,\mathrm{W\,m^{-1}\,K^{-1}}$, (Figure 4);
2. C_p constant and k decreases on temperature, (Figure 5);
3. C_p constant and k increases on temperature, (Figure 6);
4. $C_p(T)$ and k decreases on temperature, (Figure 7);
5. $C_p(T)$ and k increases on temperature, (Figure 8);

Table 1. Constant thermal properties values used in control test simulation.

Material	C_p (J kg^{-1} K^{-1})	k (W m^{-1} K^{-1})	ρ (kg m^{-3})
Gd	174.12 235.83 302.06	10.5	7900

Temperature response and the MCM's discharged energy results were plotted and analyzed in Figures 4–8, using constant thermal properties (T.P.) values of $C_p = 302.06\,\mathrm{J\,kg^{-1}\,K^{-1}}$ and $k = 10.5\,\mathrm{W\,m^{-1}\,K^{-1}}$.

For this particular case, the chosen constant scenario begins the process with higher accumulated energy, where it is easier to assess the major differences in thermal response and heat outflow for the temperature-dependent situation.

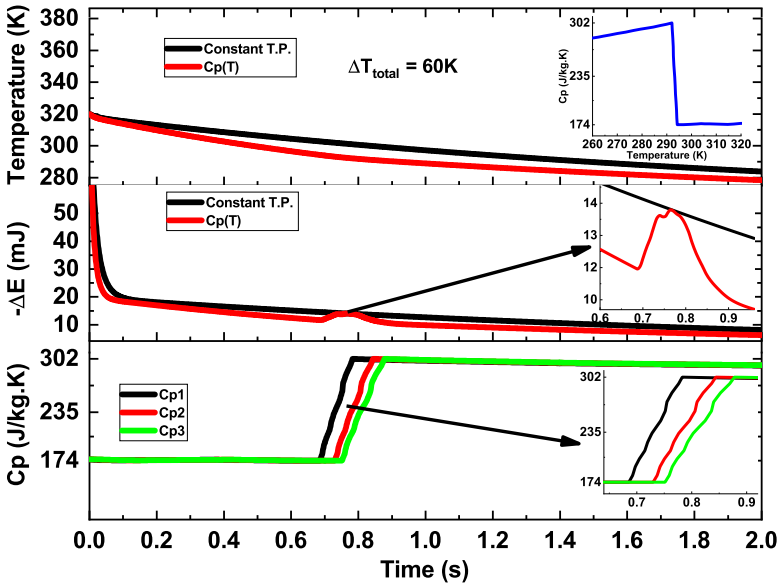

Figure 4. Nodal temperature response (**top**), discharged energy (**middle**) and $C_p(T)$ behaviour at the considered nodal points (**bottom**). Figure insets highlight the effect of C_p temperature dependency.

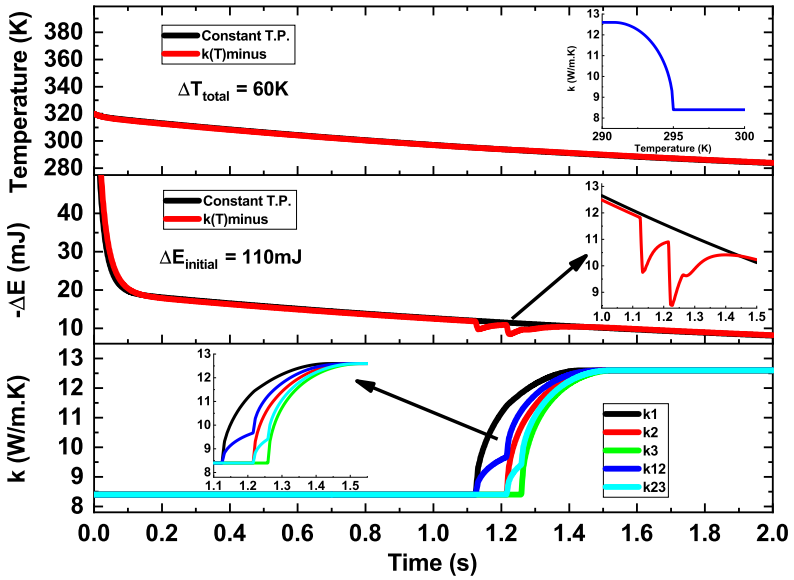

Figure 5. Nodal temperature response (**top**), discharged energy (**middle**) and $k(T)$ behaviour at the considered nodal points and at the control volumes interfaces (**bottom**). Figure insets highlight the effect of k temperature dependency.

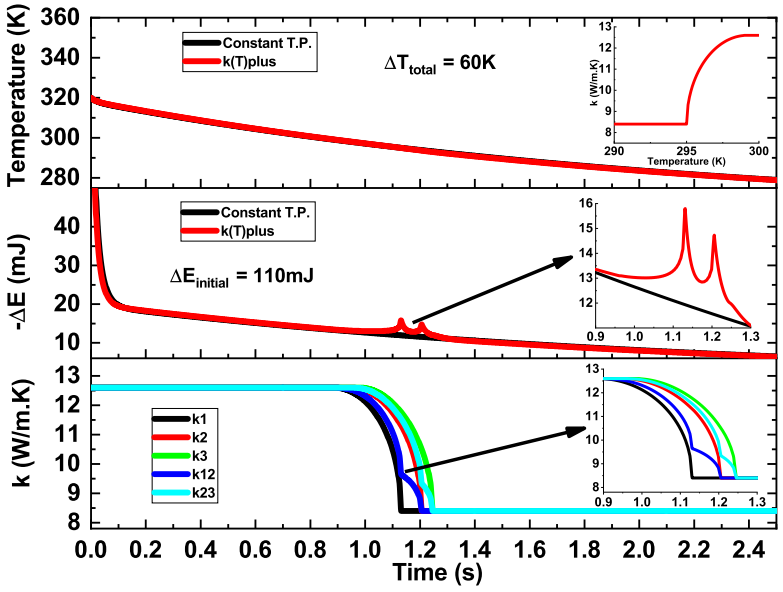

Figure 6. Nodal temperature response (**top**), discharged energy (**middle**) and $k(T)$ behaviour at the considered nodal points and at the control volumes interfaces (**bottom**). Figure insets highlight the effect of k temperature dependency.

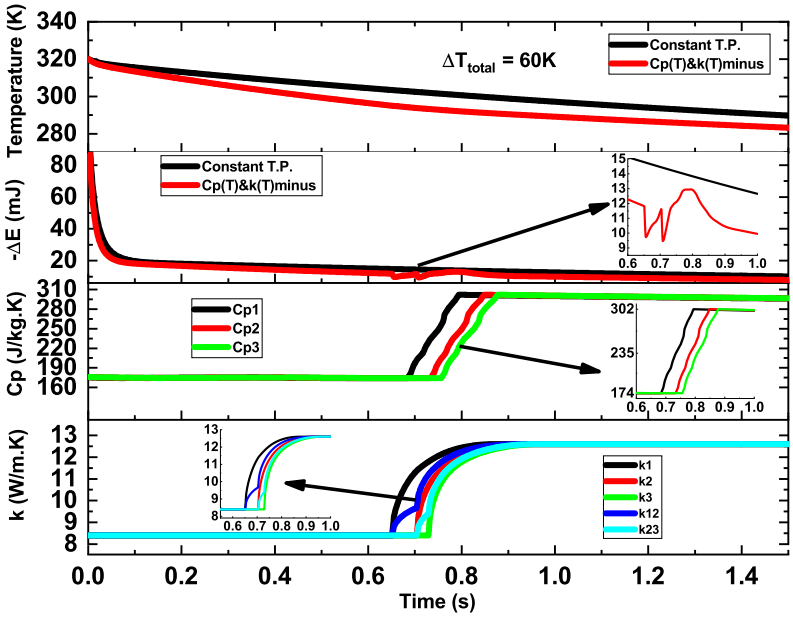

Figure 7. Nodal temperature response (**top**) and discharged energy (**middle1**). $C_p(T)$ (**middle2**) and $k(T)$ (**bottom**) behaviours at the considered nodal points and at the control volumes interfaces. Figure insets highlight the combined effects of k and C_p temperature dependencies.

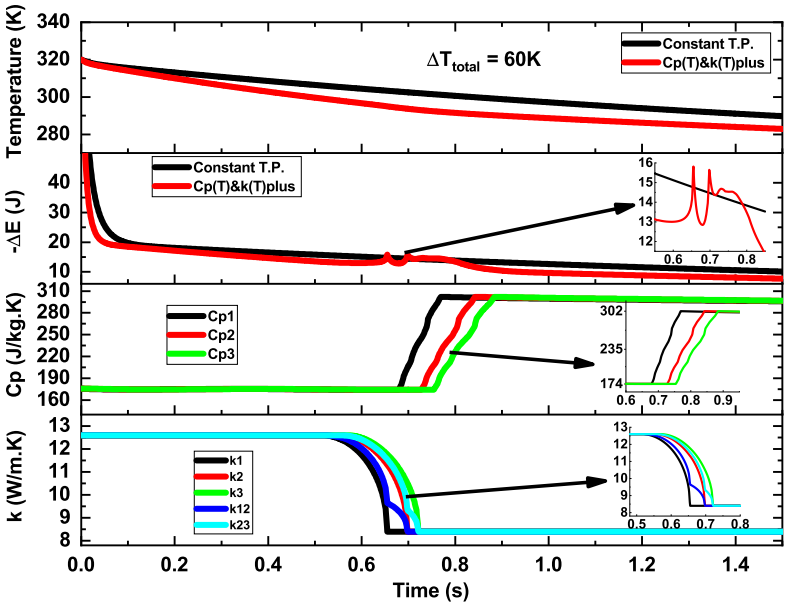

Figure 8. Nodal temperature response (**top**) and discharged energy (**middle1**). $C_p(T)$ (**middle2**) and $k(T)$ (**bottom**) behaviours at the considered nodal points and at the control volumes interfaces. Figure insets highlight the combined effects of k and C_p temperature dependencies.

Tables 2–4 highlight the difference in thermal response between the considered cases, analysing the temperature difference between control and temperature dependent models. The temperature response for the first second in a cool-down process is of significant relevance as current magnetocaloric cycle simulations consider frequencies around 1 Hz [40,41]. $\Delta T_{t=1s}$ and ΔT_{Max} represent the temperature difference for $t = 1s$ and the instant where this difference reaches its peak value, respectively.

Another essential aspect when characterizing the system's heat transfer process is the time that a given scenario takes to reach a complete temperature response (CTR). The time difference Δt_{CTR} provides us with the time between the two studied models when the system settles close to the steady-state temperature. The negative values for this time

difference indicate that the temperature dependent process is slower for fixed C_p and k values.

Figure 9 shows the normalized temperature difference for the boundary point 1.

$$\frac{T(t) - T_\infty}{T_i - T_\infty} = \frac{\Delta T(t)}{\Delta T_{Max}} \tag{7}$$

Equation (7) represents the ratio between the temperature change from the beginning for each instant t and the maximum temperature change that the system can undergo.

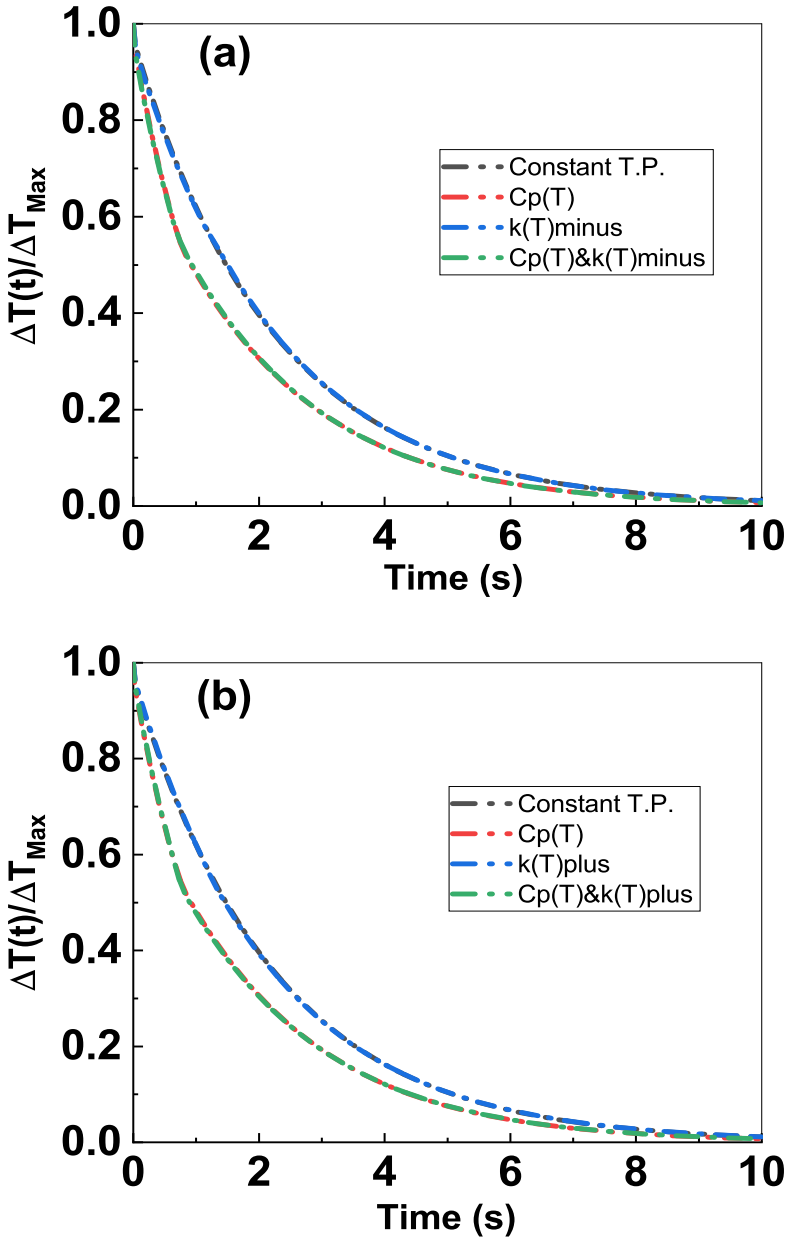

Figure 9. Normalized temperature difference results. (**a**) $k(T)minus$ and $C_p(T)$ & $k(T)minus$ against constant T.P. and $C_p(T)$ scenarios. (**b**) $k(T)plus$ and $C_p(T)$ & $k(T)plus$ against constant T.P. and $C_p(T)$ scenarios.

The normalized temperature change gives a general overlook about which thermal property affects the temperature response the most. It allows us to compare the thermal conductivity data sets, ***k(T)*minus** and ***k(T)*plus** (subplots **a** and **b**, respectively) against the $C_p(T)$ and constant T.P. scenarios,

The obtained results highlight that temperature dependent specific heat has a larger impact on the system's thermal kinetics due to changes in energy storage capacity that the material undergoes. The energy storage capacity increases during cool-down, creating a delay in heat flow at the end of the transfer process (see Figure 4—middle).

We can also infer that the system achieves a faster CTR when k increases during cool-down process (Figures 5 and 6). When considering temperature dependent k, a pattern arises between adjacent control volumes, where the thermal conductivity on each interface (k_{12} and k_{23}) behaves like a "heat gate". When k changes with temperature, each "gate" gradually opens or closes, adjusting the heat flow rate accordingly.

Table 2. $\Delta T_{t=1s}$, ΔT_{Max} and Δt_{CTR} obtained for each T.P. initial values: C_p = 302.06 J kg^{-1} K^{-1} and k = 10.5 W m^{-1} K^{-1}.

Constant T.P.	**C_p = 302.06 J kg^{-1} K^{-1}/ k = 10.5 W m^{-1} K^{-1}**				
Dynamic T.P.	$C_p(T)$	$k(T)minus$	$k(T)plus$	$C_p(T)$ & $k(T)minus$	$C_p(T)$ & $k(T)plus$
ΔT_{1s}(K)	8.25	0.18	0.10	8.03	8.50
ΔT_{Max}(K)	8.86	0.41	0.33	8.68	9.12
Δt_{CTR}(s)	1.0	0.03	−0.06	1.1	0.98

Table 3. $\Delta T_{t=1s}$, ΔT_{Max} and Δt_{CTR} obtained for each T.P. initial values: C_p = 235.83 J kg^{-1} K^{-1} and k = 10.5 W m^{-1} K^{-1}.

Constant T.P.	**C_p = 235.83 J kg^{-1} K^{-1}/ k = 10.5 W m^{-1} K^{-1}**				
Dynamic T.P.	$C_p(T)$	$k(T)minus$	$k(T)plus$	$C_p(T)$ & $k(T)minus$	$C_p(T)$ & $k(T)plus$
ΔT_{1s} (K)	3.88	0.17	0.33	3.66	4.13
ΔT_{Max} (K)	5.11	0.41	0.33	5.07	5.38
Δt_{CTR} (s)	−1.4	0.025	−0.045	−1.4	−1.4

Table 4. $\Delta T_{t=1s}$, ΔT_{Max} and Δt_{CTR} obtained for each T.P. initial values: C_p = 174.12 J kg^{-1} K^{-1} and k = 10.5 W m^{-1} K^{-1}.

Constant T.P.	**C_p = 174.12 J kg^{-1} K^{-1}/ k = 10.5 W m^{-1} K^{-1}**				
Dynamic T.P.	$C_p(T)$	$k(T)minus$	$k(T)plus$	$C_p(T)$ & $k(T)minus$	$C_p(T)$ & $k(T)plus$
ΔT_{1s} (K)	2.13	0.24	0.24	2.35	1.88
ΔT_{Max} (K)	6.21	0.42	0.33	6.28	6.16
Δt_{CTR} (s)	−3.6	0.019	−0.033	−3.6	-3.7

5. Conclusions

In this work, a 1D heat transfer model was used to simulate the cool-down process of an idealized magnetic solid refrigerant. The MCM numerical model takes into consideration not only the $C_p(T)$ function as input but also its thermal conductivity temperature dependency. The MC refrigerant constitutes the most dynamic part of any magnetic refrigeration system, and any changes in its physical properties during the device's operation should not be dismissed to more accurately predict their influence on the heat transfer processes.

The present study analyses the temperature response by segregating each considered temperature dependence ($k(T)$ and $C_p(T)$). Then it combines all the results to highlight how and why MCM numerical models should account for both thermal properties' temperature dependencies to provide a more accurate evaluation of the heat transport.

Figure 4 and Table 2 refer to the $C_p(T)$ model, which displays temperature differences of 8.25 K for the first simulated second, and 8.5 K for the maximum temperature variation. By comparing the two $k(T)$ regimes in the considered cooling process, the ***k(T)minus*** model always has the highest maximum temperature change due to a thermal conductivity increase.

When considering the temperature dependent physical properties' scenarios, the most significant variations arise when the $C_p(T)$ model is applied. By combining simultaneously the $C_p(T)$ and the $k(T)$ dependencies, the results present important incremental changes,

that can enable or hinder the material's ability to trap the accumulated thermal energy (see Figures 7 and 8).

Even in cases where a single cooling process presents slight differences in thermal response, these changes can impact significantly the complete AMR model's accuracy, as it depends on the solid refrigerant's ability to execute many heat transfer cycles with the smallest thermal response error propagation. Nevertheless, in the literature the temperature dependent thermal properties (especially the thermal conductivity k) are still ignored by most numerical reference models [18,20,38].

The results gathered in this paper were obtained through a 1D mathematical model, solved using a simple numerical code, allowing for complete control of the temperature dependent input parameters and the overall simulation process. Since a single magnetocaloric element model can change its thermal kinetics in just half a cycle, this study highlights the relevance of implementing accurate temperature dependent properties, by always considering $C_p(T)$ and $k(T)$ functions.

In AMR devices, the effects due to the thermal properties temperature dependence will be present. Beginning with a chosen set of operational parameters, these effects can have a stronger or weaker impact on the systems' performance. However, once the influence of these dependencies is known, at an elemental level, and introduced numerically into the models, it is brought to light that results can be more realistic, leading to better performance evaluations. Furthermore, the implemented simplified model can also be used for a preliminary temperature response evaluation for first and second order magnetic transition materials.

Author Contributions: Conceptualization, A.P.L. and V.A.F.C.; Investigation, A.P.L.; Methodology, V.A.F.C.; Supervision, J.S.A.; Writing—original draft, A.P.L.; Writing—review & editing, A.P.L., V.A.F.C. and J.S.A. All authors have read and agreed to the published version of the manuscript.

Funding: A. P. Lopes acknowledges a PhD grant funded by Fundação para a Ciência e Tecnologia (FCT), reference SFRH/BD/ 129340/2017. J. S. Amaral acknowledges FCT IF/01089/2015 grant. V. A. F. Costa acknowledges projects UIDB/00481/2020 and UIDP/00481/2020—FCT; and CENTRO-01-0145-FEDER-022083—Centro Portugal Regional Operational Programme (Centro2020), under the PORTUGAL 2020 Partnership Agreement, through the European Regional Development Fund. This work was developed within the scope of the project CICECO-Aveiro Institute of Materials, UIDB/50011/2020 and UIDP/50011/2020, financed by national funds through the FCT/MEC, and also developed in the scope of the Smart Green Homes Project [POCI-01-0247-FEDER-007678], a co-promotion between Bosch Termotecnologia S.A. and the University of Aveiro, financed by Portugal 2020 under the Competitiveness an Internationalization Operational Program, and by the European Regional Development Fund.

Institutional Review Board Statement: The study did not require ethical approval.

Informed Consent Statement: Not applicable.

Conflicts of Interest: The authors declare that there are no conflict of interest to disclose.

Abbreviations

C	specific heat (J kg^{-1} K^{-1})
k	thermal conductivity (W m^{-1} K^{-1})
L	material's length (m)
T	Temperature (K)
t	time (s)
x	position (m)
h	heat transfer coefficient (W m^{-2} K^{-1})
Δ	change, difference
ρ	density (kg m^{-3})
n	time index

ad	adiabatic
∞	idealized external medium
i	initial

References

1. Kitanovski, A. Energy Applications of Magnetocaloric Materials. *Adv. Energy Mater.* **2020**, *10*, 3741. [CrossRef]
2. Potočnik, P.; Vidrih, B.; Kitanovski, A.; Govekar, E. Analysis and optimization of thermal comfort in residential buildings by means of a weather-controlled air-to-water heat pump. *Build. Environ.* **2018**, *140*, 68–79. [CrossRef]
3. United Nations Secretariat. *The Importance of Energy Efficiency in the Refrigeration and Heat Pump Sectors*; Technical Report May; United Nations: Vienna, Austria, 2018.
4. Zimm, C.; Boeder, A.; Mueller, B.; Rule, K.; Russek, S.L. The evolution of magnetocaloric heat-pump devices. *MRS Bull.* **2018**, *43*, 274–279. [CrossRef]
5. Aprea, C.; Greco, A.; Maiorino, A.; Masselli, C. The employment of caloric-effect materials for solid-state heat pumping. *Int. J. Refrig.* **2020**, *109*, 1–11. [CrossRef]
6. Lei, T.; Engelbrecht, K.; Nielsen, K.K.; Veje, C.T. Study of geometries of active magnetic regenerators for room temperature magnetocaloric refrigeration. *Appl. Therm. Eng.* **2017**, *111*, 1232–1243. [CrossRef]
7. Roudaut, J.; Kedous-Lebouc, A.; Yonnet, J.P.; Muller, C. Numerical analysis of an active magnetic regenerator. *Int. J. Refrig.* **2011**, *34*, 1797–1804. [CrossRef]
8. Yu, B.; Liu, M.; Egolf, P.W.; Kitanovski, A. A review of magnetic refrigerator and heat pump prototypes built before the year 2010. *Int. J. Refrig.* **2010**, *33*, 1029–1060. [CrossRef]
9. Kitanovski, A.; Tušek, J.; Tomc, U.; Plaznik, U.; Ožbolt, M.; Poredoš, A. *Magnetocaloric Energy Conversion*, *Green Energy and Technology*; Springer International Publishing: Cham, Switzerland, 2015; Volume 179, pp. 167–210. [CrossRef]
10. Tishin, A.M.; Pecharsky, V.K.; Gschneidner, K.A. Magnetic phase transitions and the magnetothermal properties of gadolinium. *Phys. Rev. B* **1998**, *57*, 3478–3490.
11. Griffith, L.; Czernuszewicz, A.; Slaughter, J.; Pecharsky, V. CaloriSMART: Small-scale test-stand for rapid evaluation of active magnetic regenerator performance. *Energy Convers. Manag.* **2019**, *199*, 111948. [CrossRef]
12. Eriksen, D.; Engelbrecht, K.; Haffenden Bahl, C.R.; Bjørk, R. Exploring the efficiency potential for an active magnetic regenerator. *Sci. Technol. Built Environ.* **2016**, *22*, 527–533. [CrossRef]
13. Aprea, C.; Greco, A.; Maiorino, A. An application of the artificial neural network to optimise the energy performances of a magnetic refrigerator. *Int. J. Refrig.* **2017**, *82*, 238–251. [CrossRef]
14. Dall'Olio, S.; Lei, T.; Engelbrecht, K.; Bahl, C.R. Effet de l'effilage sur le lit d'un régénérateur magnétocalorique. *Int. J. Refrig.* **2017**, *84*, 300–308. [CrossRef]
15. Plait, A.; Giurgea, S.; De Larochelambert, T.; Nika, P.; Espanet, C. Low computational cost semi-analytical magnetostatic model for magnetocaloric refrigeration systems. *AIP Adv.* **2018**, *8*, 95204. [CrossRef]
16. Kitanovski, A.; Plaznik, U.; Tomc, U.; Poredoš, A. Present and future caloric refrigeration and heat-pump technologies. *Int. J. Refrig.* **2015**, *57*, 288–298. [CrossRef]
17. Bouchard, J.; Nesreddine, H.; Galanis, N. Model of a porous regenerator used for magnetic refrigeration at room temperature. *Int. J. Heat Mass Transf.* **2009**, *52*, 1223–1229. [CrossRef]
18. Kamran, M.S.; Sun, J.; Tang, Y.B.; Chen, Y.G.; Wu, J.H.; Wang, H.S. Numerical investigation of room temperature magnetic refrigerator using microchannel regenerators. *Appl. Therm. Eng.* **2016**, *102*, 1126–1140. [CrossRef]
19. Mugica, I.; Poncet, S.; Bouchard, J. An open source DNS solver for the simulation of Active Magnetocaloric Regenerative cycles. *Appl. Therm. Eng.* **2018**, *141*, 600–616. [CrossRef]
20. Silva, D.J.; Ventura, J.; Araújo, J.P. Caloric devices: A review on numerical modeling and optimization strategies. *Int. J. Energy Res.* **2021**, 1–42. [CrossRef]
21. Christiaanse, T.V.; Trevizoli, P.V.; Rowe, A. Modelling two layer Mn–Fe–Si–P materials in an active magnetic regenerator. *Int. J. Refrig.* **2019**, *106*, 225–235. [CrossRef]
22. Azad, A.; Ahmadi, P.; Geshani, H.; Wongwises, S. Parametric study of an active magnetic refrigeration (AMR) system on exergy efficiency and temperature span with Gadolinium. *J. Therm. Anal. Calorim.* **2021**, *145*, 1691–1710. [CrossRef]
23. Chdil, O.; Balli, M.; De Rango, P.; El Maalam, K.; El Boukili, A.; Mounkachi, O. Assessment of near $Pr_{2/3}Sr_{1/3}MnO_3$ oxide in magnetic cooling. *Int. J. Refrig.* **2022**, *133*, 302–312. [CrossRef]
24. Risser, M.; Vasile, C.; Muller, C.; Noume, A. Improvement and application of a numerical model for optimizing the design of magnetic refrigerators. *Int. J. Refrig.* **2013**, *36*, 950–957. [CrossRef]
25. Vuarnoz, D.; Kawanami, T. Numerical analysis of a reciprocating active magnetic regenerator made of gadolinium wires. *Appl. Therm. Eng.* **2012**, *37*, 388–395. [CrossRef]
26. Burdyny, T.; Ruebsaat-Trott, A.; Rowe, A. Performance modeling of AMR refrigerators. *Int. J. Refrig.* **2014**, *37*, 51–62. [CrossRef]
27. Qian, S.; Yuan, L.; Yu, J.; Yan, G. Critical parameters in design of active magnetocaloric regenerators for magnetic refrigeration applications. *Int. J. Refrig.* **2017**, *84*, 151–164. [CrossRef]
28. Nielsen, K.K.; Engelbrecht, K. The influence of the solid thermal conductivity on active magnetic regenerators. *J. Phys. D Appl. Phys.* **2012**, *45*, 14. [CrossRef]

29. Silva, D.; Davarpanah, A.; Amaral, J.; Amaral, V. Temperature dependent thermal conductivity of magnetocaloric materials: Impact assessment on the performance of active magnetic regenerative refrigerators. *Int. J. Refrig.* **2019**, *106*, 181–187. [CrossRef]
30. Fujieda, S.; Hasegawa, Y.; Fujita, A.; Fukamichi, K. Thermal transport properties of magnetic refrigerants $La(Fe_xSi_{1-x})_{13}$ and their hydrides, and Gd_5 Si_2 Ge_2 and MnAs. *J. Appl. Phys.* **2004**, *95*, 2429–2431. [CrossRef]
31. Porcari, G.; Morrison, K.; Cugini, F.; Turcaud, J.A.; Guillou, F.; Berenov, A.; Van Dijk, N.H.; Brück, E.H.; Cohen, L.F.; Solzi, M. Influence of thermal conductivity on the dynamic response of magnetocaloric materials. *Int. J. Refrig.* **2015**, *59*, 29–36. [CrossRef]
32. Maiorino, A.; Del Duca, M.G.; Tušek, J.; Tomc, U.; Kitanovski, A.; Aprea, C. Evaluating Magnetocaloric Effect in Magnetocaloric Materials: A Novel Approach Based on Indirect Measurements Using Artificial Neural Networks. *Energies* **2019**, *12*, 1871. [CrossRef]
33. Aprea, C.; Greco, A.; Maiorino, A.; Masselli, C. Energy performances and numerical investigation of solid-state magnetocaloric materials used as refrigerant in an active magnetic regenerator. *Therm. Sci. Eng. Prog.* **2018**, *6*, 370–379. [CrossRef]
34. Monfared, B.; Palm, B. Material requirements for magnetic refrigeration applications. *Int. J. Refrig.* **2018**, *96*, 25–37. [CrossRef]
35. Ucar, H.; Paudyal, D.; Boyraz, O. Using numerical methods to screen magnetocaloric materials in an active magnetic regenerative cycle. *Int. J. Refrig.* **2020**, *120*, 50–57. [CrossRef]
36. Petersen, T.F.; Pryds, N.; Smith, A.; Hattel, J.; Schmidt, H.; Høgaard Knudsen, H.J. Two-dimensional mathematical model of a reciprocating room-temperature Active Magnetic Regenerator. *Int. J. Refrig.* **2008**, *31*, 432–443. [CrossRef]
37. Lionte, S.; Vasile, C.; Siroux, M. Numerical analysis of a reciprocating active magnetic regenerator. *Appl. Therm. Eng.* **2015**, *75*, 871–879. [CrossRef]
38. Eustache, J.; Plait, A.; Dubas, F.; Glises, R. Review of Multi-Physics Modeling on the Active Magnetic Regenerative Refrigeration. *Math. Comput. Appl.* **2021**, *26*, 47. [CrossRef]
39. Incropera, F.P. *Fundamentals of Heat and Mass Transfer*; Wiley: Hoboken, NJ, USA, 2011; Volume 33, pp. 1–27.
40. Mugica, I.; Poncet, S.; Bouchard, J. Detailed numerical simulations of a single stage of rotatory active magnetic regenerators: Influence of the pin geometry. *Int. J. Therm. Sci.* **2020**, *149*, 106198. [CrossRef]
41. Krautz, M.; Beyer, L.; Funk, A.; Waske, A.; Weise, B.; Freudenberger, J.; Gottschall, T. Predicting the dominating factors during heat transfer in magnetocaloric composite wires. *Mater. Des.* **2020**, *193*, 108832. [CrossRef]